Journal of Applied Polymer Science

Photoactivity of Poly(lactic acid) Nanocomposites Modulated by TiO_2 Nanofillers

Yonghui Li,[1] Caihong Chen,[2,3] Jun Li,[2] Xiuzhi Susan Sun[1]

[1]Bio-materials and Technology Lab, Department of Grain Science and Industry, Kansas State University, Manhattan, Kansas 66506

[2]Department of Chemistry, Kansas State University, Manhattan, Kansas 66506

[3]School of Chemistry and Chemical Engineering, South China University of Technology, Guangzhou 510640, People's Republic of China

Correspondence to: X. S. Sun (E-mail: xss@ksu.edu)

ABSTRACT: Photoactivity of poly(lactic acid) (PLA) nanocomposites is of great interest for rational design of products for either short-term/single-use or long-term/durable applications. We prepared PLA/TiO_2 nanocomposite films through a solution mixing/film casting method. Results showed that photodegradability/photostability of PLA could be well modulated by selecting appropriate TiO_2 nanofillers. TiO_2 nanoparticles and nanowires were characterized using X-ray diffraction, UV–Vis–NIR spectrophotometer, and scanning electron microscopy. Changes in color, weight, structure, thermal stability, and phase transitions of PLA and nanocomposite films before and after UV irradiation were evaluated to study photoactivity characteristics. Pure PLA exhibited moderate photodegradability, but the photodegradability and photostability of PLA nanocomposites (PNA) were significantly enhanced by NanoActive (NA) TiO_2 nanoparticles and A type TiO_2 nanowires, respectively. Pure PLA had a weight loss of 27% after 38 days of UV irradiation. The weight loss of photodegradable (PD) PNA (PNA = PLA with 1% NA TiO_2) reached 38%, whereas that of photostable (PS) nanocomposites (P3AW) (P3AW = PLA with 3% A type TiO_2 nanowire) was only 5%. PD PLA exhibited characteristic peaks of carboxylic acid OH stretching and C=C double bond after UV irradiation in Fourier-transform infrared spectra, whereas spectra of PS PLA remained almost the same. Thermal decomposition temperatures, glass transition temperatures, and melting temperatures of PD PLAs decreased dramatically after UV irradiation, but no obvious changes were observed for those of PS PLAs. © 2013 Wiley Periodicals, Inc. J. Appl. Polym. Sci. **2014**, *131*, 40241.

KEYWORDS: biopolymers and renewable polymers; differential scanning calorimetry (DSC); thermal properties; nanoparticles; nanowires and nanocrystals; composites

Received 17 October 2013; accepted 3 December 2013

DOI: 10.1002/app.40241

INTRODUCTION

Plastic products based on petroleum-derived polymers have been serving our needs for many decades, but we are facing severe environmental issues as well as a petroleum resource crisis. Consequently, the development of alternative and biodegradable plastics from renewable resources has attracted much attention. Poly(lactic acid) (PLA), originating from renewable sugar-based resources, has shown great potential to produce biodegradable plastics.[1–4] PLA plastics usually experience moderate photodegradation under ultraviolet (UV) irradiation,[5–7] but the rate is considered relatively slow for most short-term and single-use products. Besides, although PLA products are biodegradable, biodegradation advances only when moisture and bacteria exist, and it takes relatively long time.[8] In contrast, photodegradation of PLA could occur under any conditions in which UV irradiation is available. The combination of biodegradation and photodegradation would greatly benefit waste treatment of those products after usage. On the other hand, for durable outdoor applications, photodegradation of PLA must be inhibited. Therefore, it is necessary to develop PLA materials with modulated photoactivity; specifically, materials need either further accelerated photodegradability or enhanced photostability so PLA products for various usages can be rationally designed to expand their applications.

TiO_2 exists as two main polymorphs: anatase and rutile. TiO_2 possesses a wide band gap (e.g., ~3.2 eV for anatase phase and ~3.0 eV for rutile phase), which makes its polymorphs capable of absorbing UV light ($\lambda < 384$ nm for anatase and <410 nm for rutile).[9] Some researchers believe the photocatalytic performance of anatase is superior to that of rutile, because the

larger grain size of rutile leads to lower capacity to absorb water and oxygen, and a higher rate of electron–hole recombination.[9,10] However, this conclusion may not be true unless the two phases are compared at the same grain size. Rutile also has been reported to have a higher surface enthalpy and higher surface free energy than anatase.[11] Hence, the wetting capacity of rutile by water would be expected to be superior to that of anatase[9] and lead to more free radicals, which would result in a better photocatalytic performance. Excellent photocatalytic activity of rutile TiO_2 has been reported.[12] Mixed-phase TiO_2 with both rutile and anatase compositions has been reported to exhibit enhanced photoactivity compared with single-phase TiO_2.[13] The enhanced photoactivity is considered to be a result of improved charge carrier separation, possibly through the trapping of electrons in one phase and the consequent reduction in electron–hole recombination.[14] A study compared the photocatalytic activity of amorphous and anatase TiO_2, and found that the photocatalytic activity of anatase is appreciable, whereas that of amorphous TiO_2 was negligible.[15] A few studies have been conducted on the photocatalytic activity of polymer/TiO_2 nanocomposites, including polystyrene,[16] polyethylene,[17] poly(butylenes succinate),[18] and polyurethane.[19]

Pure PLA absorbs UV light below 295 nm due to the C═O chromophore, which induces photodegradation by a Norrish II mechanism of carbonyl polyester.[5] Using TiO_2 nanoparticles as fillers in PLA matrix may alter the photoactivity mechanism. The TiO_2 nanoparticles may play two roles: (1) blocking UV light below 295 nm wavelength, thus reducing the natural photodegradation of PLA; and (2) generating radical oxidation at the TiO_2 surface due to photo-induced electron/hole separation in TiO_2 nanoparticles. The latter mechanism may be enhanced or suppressed depending on many factors including TiO_2 polymorph/phase composition, size, shape, dopant, surface characteristics, etc., providing a means to modulate the photoactivity of the composites.

In this study, we employed different types of TiO_2 nanofillers (nanoparticles and nanowires) and synthesized PLA/TiO_2 nanocomposites via solution mixing and film casting. The objectives of this study were to develop photodegradable (PD) and photostable (PS) PLA nanocomposites (PNA), respectively, and to investigate their photoactivity characteristics. Changes in color, weight, structure, thermal stability, and phase transitions of nanocomposite films before and after UV irradiation were evaluated.

EXPERIMENTAL

Materials

PLA (2002D) in pellet form was supplied by NatureWorks LLC (Minnetonka, MN). NanoActive TiO_2 nanoparticles (NA TiO_2) were obtained from NanoScale Co. (Manhattan, KS). NA TiO_2 is made from tiny crystals (<2 nm) embedded in the amorphous matrix and has a specific surface area larger than 500 $m^2\ g^{-1}$ as reported by the manufacture. TiO_2 nanoparticles of mixed phase (SA TiO_2, <100 nm, mixture of rutile and anatase TiO_2) were purchased from Sigma-Aldrich. Chloroform, sodium hydroxide (NaOH), and hydrochloric acid (HCl) were obtained from Fisher Scientific. Absolute ethanol was obtained from Decon Laboratories.

Synthesis of TiO_2 Nanowires

TiO_2 nanowires were synthesized according the method described in Ref. 20. For a typical preparation, 0.1 g SA TiO_2 nanoparticles were placed into a Teflon-lined autoclave of 50-mL capacity. It was then filled with 40 mL 10*M* NaOH aqueous solution, sealed into a stainless steel tank, and maintained at 200°C for 24 hr. After cooling, the sample was washed with 1*M* aqueous HCl solution, deionized water, and absolute ethanol several times in sequence, then dried in a vacuum oven at 80°C for 12 hr to obtain type A TiO_2 nanowires. Type B TiO_2 nanowires were obtained by calcinating type A TiO_2 nanowires in a Muffle furnace at 800°C for 12 hr. Both type A and B TiO_2 nanowires are white and soft, and fibrous in form.

Characterization of TiO_2 Nanowires

The powder X-ray diffraction (XRD) patterns were recorded on a Bruker D8 X-ray diffractometer with Cu-$K\alpha$ radiation. The scans ranged from 10° to 90°, with a scanning rate of 6° min^{-1}. The optical properties of the synthesized TiO_2 nanowires were measured on a UV–Vis–NIR spectrophotometer (Varian Cary 500 Scan) in diffuse reflection mode, and at least two replicates were performed. The morphology of the nanowires was observed using scanning electron microscopy (SEM, Hitachi S-3500N, Hitachi Science Systems, Ltd., Japan). The samples were glued to aluminum specimen mounts and coated with a mixture of 60% gold particles and 40% palladium with a sputter coater (Desk II Sputter/Etch Unit; Denton Vacuum, LLC; Moorestown, NJ) before SEM observation.

Preparation of PNA Films

PNA films containing 1% of various TiO_2 nanoparticles (NA TiO_2 and SA TiO_2) and nanowires (A TiO_2 and B TiO_2) were prepared using a solution-mixing/film-casting technique. For a typical process, 0.02 g TiO_2 was added to 20 mL chloroform, and the mixture was sonicated for 30 min to achieve a uniform dispersion. Meanwhile, 2 g PLA was dissolved in another 20 mL chloroform. The PLA solution and TiO_2 dispersion were mixed and stirred for 1 hr and sonicated for an additional 1 hr. The mixture was cast onto a petri dish at room temperature, kept in a fume hood with controlled evaporation of the solvent for 1 week, then dried in a vacuum oven for 24 hr at 80°C to evaporate any residual solvent. Nanocomposite films with a thickness of about 100 μm were eventually obtained. Pure PLA film and PNA film containing 3% type A TiO_2 nanowires were prepared similarly. Pure PLA, PLA/1% NA TiO_2 nanoparticles, PLA/1% SA TiO_2 nanoparticles, PLA/1% A type TiO_2 nanowires, PLA/3% A type TiO_2 nanowires, and PLA/1% B type TiO_2 nanowires are referred to hereinafter as PLA, PNA, PSA, PAW, P3AW, and PBW, respectively. Distribution of nanoparticles and nanowires in the nanocomposite films was examined with an Olympus BX50 microscope.

UV Irradiation of PNA Films

Nanocomposite films were cut into 1.25 cm × 1.25 cm pieces and irradiated under an UV lamp with a primary wavelength of 254 nm and light intensity of 2300 $\mu W\ cm^{-2}$ at 2″ distance within a chamber (Cole-Parmer, Vernon Hills, IL). The films

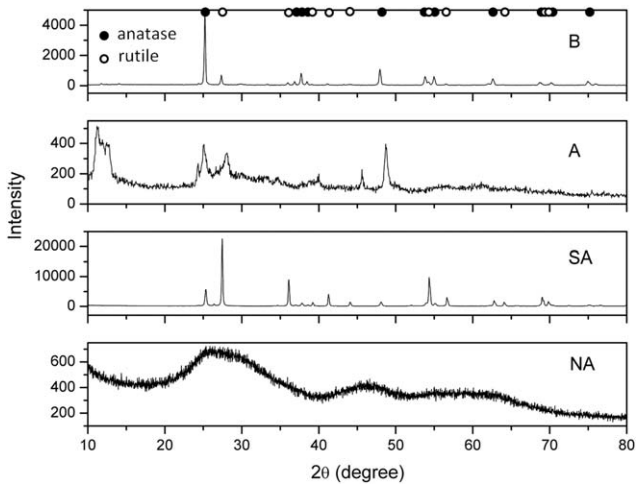

Figure 1. XRD spectra of as-received NA and SA nanoparticles and synthesized nanowires A and B. Characteristic anatase and rutile 2θ peaks are marked along the top abscissa with filled and unfilled circles for clarity, respectively.

were weighed every 4 days by an accurate balance to evaluate photodegradation/photostability. At least three replicates were conducted for each sample type. Color changes in nanocomposite films during irradiation as observed by naked eyes were recorded. After completion of irradiation (38 days), the samples (PLA, PNA, PSA, PAW, P3AW, and PBW) were collected and denoted as PLA′, PNA′, PSA′, PAW′, P3AW′, and PBW′, respectively.

Fourier-transform Infrared (FTIR) Spectroscopy

FTIR spectra of the samples before and after UV irradiation were acquired with a PerkinElmer Spectrum 400 FT-IR/FT-NIR Spectrometer (Waltham, MA). Spectra were collected in the region of 4000–400 cm^{-1} with a spectral resolution of 4 cm^{-1} and 16 scans co-added.

Thermogravimetric Analysis (TGA)

Thermal stability of the samples before and after irradiation was determined with a PerkinElmer Pyris1 TGA (Norwalk, CT). About 5 mg of each sample was placed in a platinum pan and heated from 40°C to 700°C at a heating rate of 20°C min^{-1} under nitrogen atmosphere.

Differential Scanning Calorimetry (DSC) Analysis

Thermal transitions of the samples before and after irradiation were measured using a TA DSC Q200 instrument. About 5 mg of each sample was sealed in a standard aluminum pan. An empty sealed pan was used as a reference. The sample was heated from 0°C to 190°C at a rate of 10°C min^{-1} in an inert environment by nitrogen with a gas flow rate of 50 mL min^{-1}. Heat capacity (ΔC_p), glass transition temperature (T_g), melting temperature (T_m), and heat of melting (ΔH_m) were determined from DSC thermograms. T_g was calculated from the half-width midpoint in the step change between the onset and the end temperatures of the transition. Degree of crystallinity (X_m) was estimated according to the following eq. (1):

$$X_m(\%) = \frac{\Delta H_m}{\Delta H_0 \times X_{\mathrm{PLA}}} \times 100 \quad (1)$$

where ΔH_m and ΔH_0 are heats (J g^{-1}) of melting of PNA and of PLA crystals of infinite size with a value of 93.6 J g^{-1},[21] respectively, and X_{PLA} is the PLA fraction in the bulk nanocomposites.

RESULTS AND DISCUSSION

Characteristics of TiO_2 Nanoparticles and Nanowires

Characteristic anatase and rutile 2θ peaks of TiO_2 nanoparticles and nanowires used in this study are marked along the top abscissa with filled and unfilled circles for clarity, respectively (Figure 1). NA TiO_2 yields extremely broad diffraction peaks, confirming that it is mainly in amorphous form embedded with a small amount of tiny crystals (<2 nm). SA TiO_2 exhibits both anatase and rutile patterns. The area of rutile peaks is much larger than that of the anatase peaks, indicating that SA TiO_2 is dominated by the rutile phase. The diffraction peaks of nanowire A are very broad and weak, which suggested the existence of small crystals of approximately 10–20 nm in size and amorphous phase in the nanowires.[22] The peaks from anatase phase are larger than the peaks of rutile. Calcination has been known as a common treatment to improve crystallinity of TiO_2 powders.[23,24] After calcination of nanowire A at 800°C for 12 hr, the XRD peaks of obtained nanowire B are much stronger than those of A, implying the transformation of amorphous phase to crystal phase. Moreover, the anatase peaks are much stronger than the rutile peaks in nanowire B, showing that it was dominated by the anatase phase.

The UV–vis extinction spectra of various TiO_2 nanoparticles and nanowires are shown in Figure 2. UV-absorption is a natural attribute of TiO_2 and explained by the solid band theory.[25] The onset of the UV–vis extinction for SA TiO_2 nanoparticles is at 410 nm, corresponding to the band energy of 3.0 eV for the rutile phase. The onset in the extinction curve of A and B TiO_2 nanowires derived from SA TiO_2 nanoparticles blue-shifts to about approximately 380 nm, in comparison with SA TiO_2,

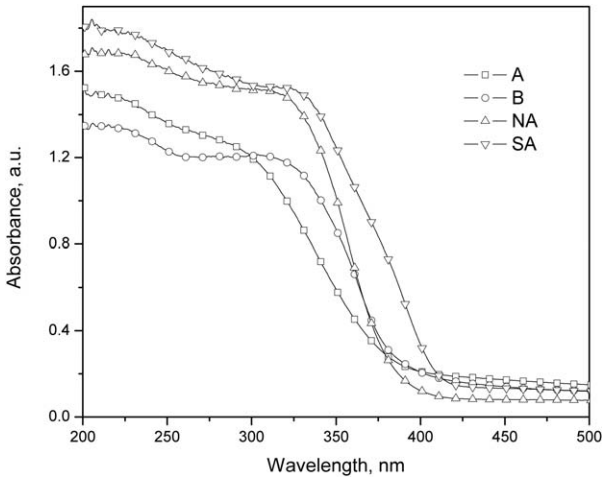

Figure 2. Typical UV–vis spectra of TiO_2 nanoparticles. NA: NanoActive TiO_2 nanoparticles; SA: Sigma-Aldrich TiO_2 nanoparticles; A: Type A TiO_2 nanowires; B: Type B TiO_2 nanowires.

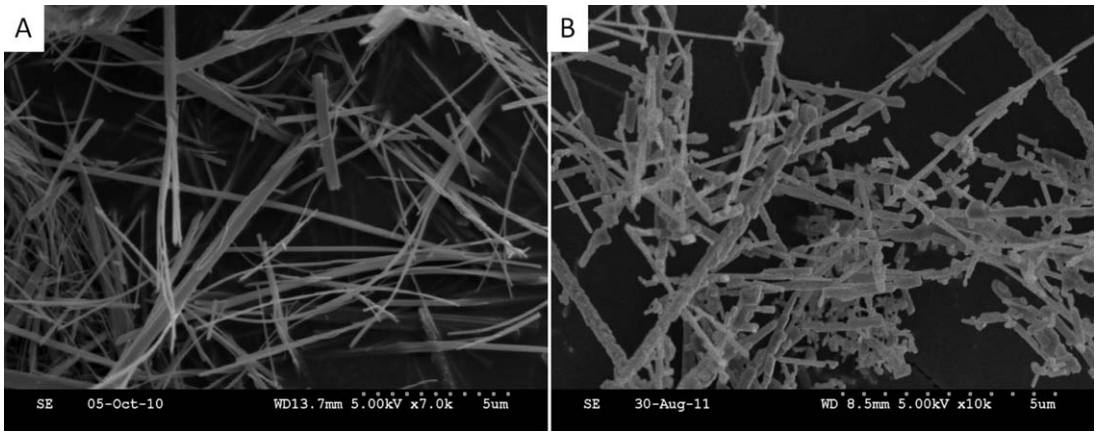

Figure 3. SEM images of synthesized TiO_2 nanowires before (A) and after (B) calcination.

which further confirms that anatase phase is dominated in the nanowires. The intensity of UV extinction of SA is stronger than that of A or B. The spectrum of the type B nanowire is slightly steeper compared with the type A nanowire, whereas the extinction of B is slightly weaker at UV wavelength lower than 300 nm. NA nanoparticles exhibit stronger UV extinction than A and B, with a threshold at about approximately 390 nm.

The A type TiO_2 nanowires exhibit a clean and smooth surface [Figure 3(A)]. The diameter is about 50–100 nm, and length varies from a few micrometers to about 20 μm, which is consistent with the literature.[20] Nanowires after calcination (B type) display a rough and irregular surface [Figure 3(B)]. The significantly different surface morphology before and after calcination was caused by the transition of amorphous phase and irregular crystals to more regular crystals during calcination.

Photodegradability/Photostability of PNA

Both nanoparticles and nanowires are distributed evenly in the PLA matrix (Figure 4); however, slight aggregations of those nanofillers are also observed due to their hydrophilic nature. Photodegradation of polymers is usually accompanied by discoloration. Pure PLA film was initially colorless, but it became yellowish after completion of irradiation. All PNA films exhibited white color before UV irradiation, as TiO_2 particles are well-known white pigments. After completion of irradiation, the color of PNA became yellow brown, but other nanocomposites remained white. The significant color change in PLA and PNA implies that more severe photodegradation occurred for those two types of samples compared with the others.

Weight loss of samples during UV irradiation is also an important direct indication of UV degradability/stability.[17,18] The weight of pure PLA and its nanocomposite films decreased linearly as UV irradiation time increased due to photodegradation (Figure 5); however, the extent of degradation varies greatly among the samples. The weight loss of pure PLA was about 27% after 38 days of irradiation. With 1% NA TiO_2 nanoparticles (PNA), the photodegradation was significantly accelerated, showing 38% weight loss in 38 days. On the other side, with 1% SA nanoparticles (PSA), photodegradation of PLA was obviously inhibited, and the weight loss was only 17.5% in the same irradiation period. The weight loss curve of nanocomposite with 1% B type TiO_2 nanowires (PBW) almost overlapped with PSA. The photodegradation of PNA with 1% A type TiO_2 nanowires (PAW) was further inhibited, with only 11% weight loss during 38 days of irradiation. When A type TiO_2 nanowire loading increased to 3%, P3AW nanocomposites exhibited stronger photostability, losing only 5% weight in 38 days.

Photodegradation of polymers under UV irradiation usually proceeds in two ways, either through chromophore groups in polymer chains, or through free radicals generated by additives or impurities in the polymer matrix. The carbonyl groups (C═O) in PLA could absorb UV irradiation, leading to PLA chain cleavage.[7,26] The photodegradation of pure PLA proceeds

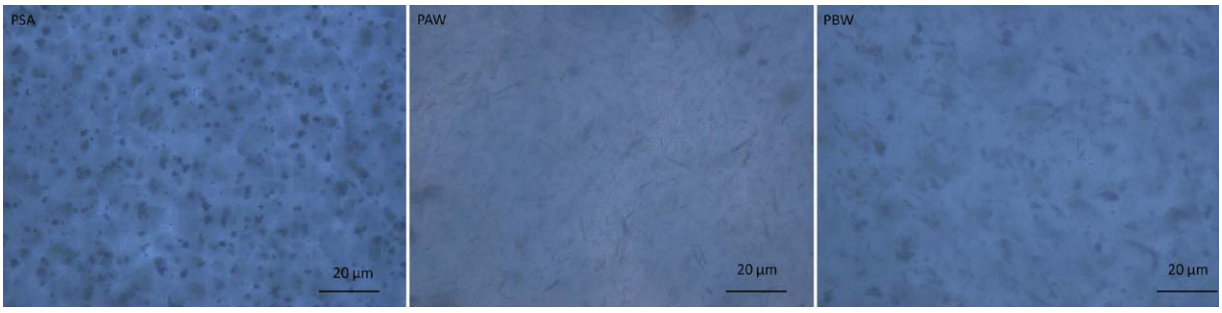

Figure 4. Microscope images of PNA films (PSA, PAW, and PBW). [Color figure can be viewed in the online issue, which is available at wileyonlinelibrary.com.]

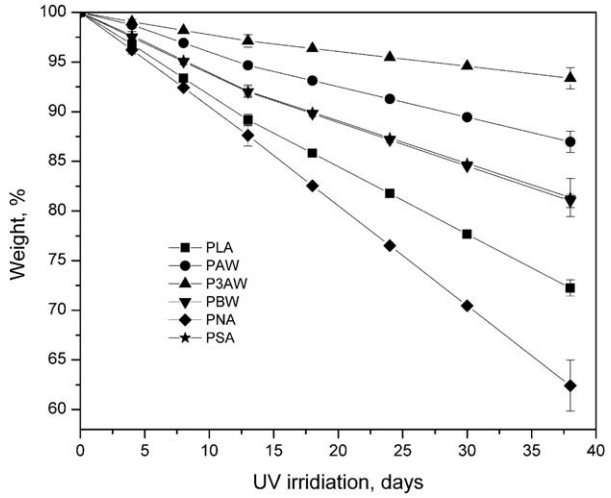

Figure 5. Weight change in pure PLA and PLA nanocomposites under UV irradiation.

via the Norrish II mechanism through the formation of C=C double bonds, as shown below[5]:

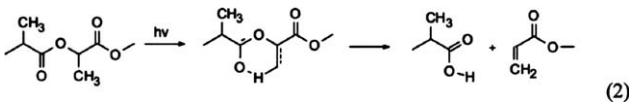

(2)

Significantly enhanced photodegradability of PNA was attributed to the incorporated small size/high surface area NA TiO_2 nanoparticles. It was reported that TiO_2 crystals of <10 nm showed significant enhancement in photocatalytic reactivity, which can be ascribed to the quantum size effect.[27] Upon UV irradiation, TiO_2 nanoparticles generate electron–hole pairs.[28] The electron–hole pairs can either recombine in the bulk or travel up to the nanoparticle surface, where they tend to activate oxygen species at the surface; for example, O_2-, HOO·, OH· radicals from H_2O or O_2 by oxidative or reductive reductions. These active oxygen species lead to further degradation reactions by attacking interfacial PLA chains, forming carbon-centered radicals, and accelerating chain cleavage through producing species such as carboxyl groups. NA TiO_2 nanoparticles possess very tiny crystal size (<2 nm) and super-high surface area (~500 m^2 g^{-1}), which allows more electrons and holes to travel to the crystal surface in generating oxygen species, leading to accelerated photodegradation of PNA.

The inhibited photodegradation of PSA and PBW was probably caused by competition of PLA and SA nanoparticles or B type nanowires absorbing UV photons. Under UV irradiation, some UV photons were absorbed by the nanoparticles or nanowires in generating electrons and holes. Due to their much larger size and smaller surface area compared with NA nanoparticles, however, the majority of generated electrons and holes recombined in the bulk before travelling to the surface, resulting in fewer free radicals to attack PLA chains. For PAW, besides the electrons and holes recombination, the trititanate impurities and amorphous components in A type nanowires provide extra sites to trap the electrons and holes,[29] leading to generation of even fewer radicals.

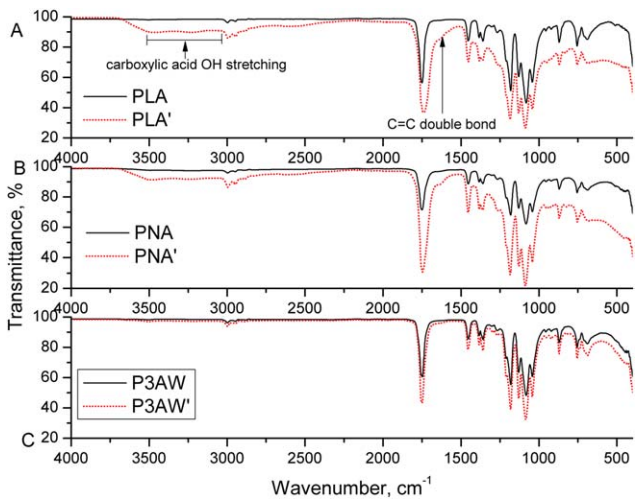

Figure 6. FTIR spectra of typical samples before (A-PLA, B-PNA, and C-P3AW) and after (A-PLA′, B-PNA′, C-P3AW′) UV irradiation. [Color figure can be viewed in the online issue, which is available at wileyonlinelibrary.com.]

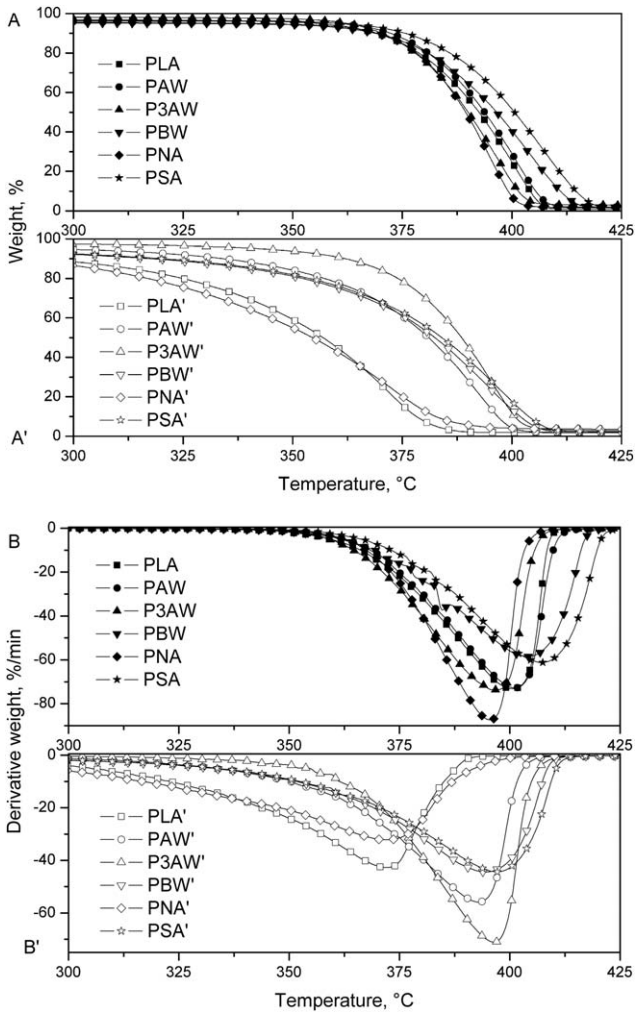

Figure 7. TGA (A, A′) and derivative TGA (B, B′) thermograms of PLA and nanocomposites before (A, B) and after (A′, B′) UV irradiation.

Table I. Thermal Decomposition Temperatures of PLA and its Nanocomposites Before and After UV Irradiation Derived From TGA Thermograms

	Before UV irradiation			After UV irradiation		
Sample	T_{onset} (°C)	T_{end} (°C)	T_{max} (°C)	T_{onset} (°C)	T_{end} (°C)	T_{max} (°C)
PLA	369.9	408.9	400.5	332.8	386.4	371.9
PNA	369.4	402.8	395.4	320.2	389.9	372.0
PSA	376.8	420.9	407.1	350.9	410.9	397.2
PBW	380.9	417.2	403.9	355.2	409.0	394.5
PAW	370.7	409.9	401.1	356.9	402.0	393.0
P3AW	366.0	405.4	396.4	365.9	405.5	396.3

There is also a possibility that the excited C═O bond generated by UV absorption in PLA may be quenched through electron transfer to TiO_2. Therefore, the photodegradation of PAW was further inhibited compared with PBW. With 3% A type TiO_2 nanowires, nanowires dominated in absorbing UV photos, and direct absorption of UV photos by PLA chains was minimal, which leads to the excellent photostability of P3AW.

FTIR

Compared with PLA, new peaks in the spectrum of PLA′ were seen at 3000–3300 cm^{-1} and 1610 cm^{-1}, which are due to carboxylic acid OH stretching and C═C double bond, respectively (Figure 6). Appearance of carboxylic acid OH group and the C═C double bond further confirms the Norrish II type photodegradation mechanism of PLA. The spectrum of PNA′ was similar to that of PLA′, indicating similar chain scission mechanisms of PLA and PNA. No new peaks were observed for P3AW′ compared with P3AW, implying minimal photodegradation of P3AW. FTIR results further confirm the excellent photodegradability and photostability of PNA containing NA TiO_2 nanoparticles and type A TiO_2 nanowires, respectively.

Thermal Properties

PLA exhibited an onset decomposition temperature (T_{onset}) of 370°C and maximum (T_{max}) and end (T_{end}) decomposition temperatures of 401°C and 409°C, respectively (Figure 7; Table I). The T_{onset}s of PSA and PBW increased by 7°C and 11°C compared with PLA, respectively, whereas the T_{onset} of PNA and PAW remained the same as PLA. The T_{onset} of P3AW decreased slightly to 366°C. The changes in thermal stability of

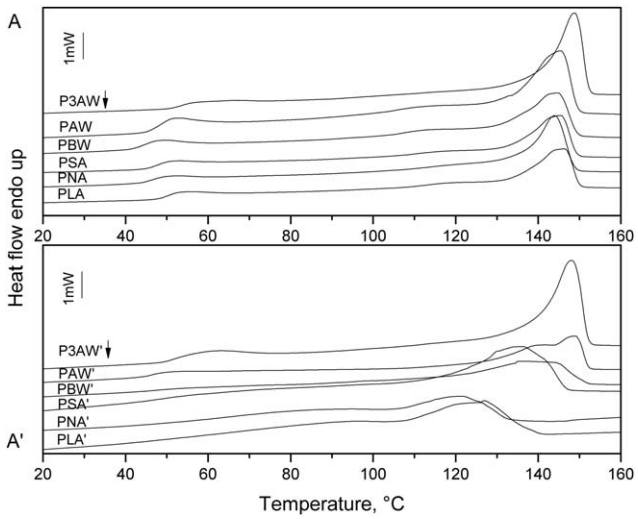

Figure 8. DSC thermograms of PLA and nanocomposites before (A) and after (A′) UV irradiation.

PNA containing TiO_2 nanoparticles and nanowires compared with pure PLA were caused by two possible competing effects: (1) the incorporated nanofillers could act as superior insulators and mass transport barriers to the volatile products generated during decomposition and improve the apparent thermal stability of nanocomposites; and (2) the TiO_2 nanofillers possess surface hydroxyl groups, which could catalyze the thermal decomposition of PLA at elevated temperatures. The different sizes, shapes, and availability of surface hydroxyl groups of TiO_2 nanofillers lead to various thermal decomposition characteristics of the nanocomposites.

After UV irradiation, T_{onset} of PLA′ was decreased by 37°C compared with that of PLA, corresponding to the irradiation-induced PLA chain scission and decreased molecular weight. The thermal decomposition decrement of PNA′ was even more significant, with T_{onset} reduced by 50°C, which was in good agreement with the accelerated photodegradability of PNA. T_{onset} decrements of PSA′ and PBW′ were about the same (26°C), corresponding to the same photodegradation extent of PSA and PBW as shown in Figure 5. T_{onset} decrement of PAW′ was only 14°C due to its enhanced photostability. P3AW′ exhibited exactly the same decomposition temperatures as P3AW, indicating no obvious thermal stability changes during UV irradiation.

Table II. Thermal Properties of PLA and its Nanocomposites Before and After UV Irradiation Determined From DSC Thermograms

	Before UV irradiation					After UV irradiation				
Sample	T_g (°C)	ΔC_p (J g^{-1} °C^{-1})	T_m (°C)	ΔH_m (J g^{-1})	X_m (%)	T_g (°C)	ΔC_p (J g^{-1} °C^{-1})	T_m (°C)	ΔH_m (J g^{-1})	X_m (%)
PLA	50.0	0.32	146.4	19.9	21.5	—	—	127.0	18.4	19.9
PNA	46.7	0.27	143.9	31.8	34.3	—	—	121.8	17.2	18.6
PSA	47.5	0.35	145.4	30.1	32.5	—	—	136.6	31.3	33.8
PBW	43.8	0.27	144.7	31.3	33.8	—	—	136.4	33.4	36.0
PAW	47.4	0.34	145.6	29.2	31.5	47.0	0.30	148.9	30.1	32.5
P3AW	54.1	0.31	148.8	34.4	37.9	53.0	0.30	148.0	31.2	34.4

The TGA results of PLA and nanocomposites before and after UV irradiation are in good agreement with the weight change, demonstrating that thermal stability characterization would be another good tool to study photodegradation.

PLA showed a T_g of 50°C, T_m of 146°C, and X_m of 21.5% (Figure 8; Table II). T_g of PNA, PSA, PBW, and PAW decreased by 2°C–6°C compared with PLA. A similar phenomenon was observed for polystyrene/silica nanocomposites.[30] Results were explained by the nonwetting nature of the untreated nanoparticle surface of polymers.[30] In the case of P3AW, T_g increased to 54°C, which was probably due to restricted PLA chain mobility by a high concentration of nanowires (3%). The T_m of all the nanocomposites ranged from 144°C to 149°C, close to that of PLA. All PNA had higher X_m than PLA, which could be explained by the fact that the nanofillers acted as extra nucleation sites for the forming of crystalline lamellar. After UV irradiation, the T_gs of PLA′, PNA′, PSA′, and PBW′ disappeared above room temperature, implying that the chain scission of these samples during UV irradiation was severe. For the same reason, the T_ms of these samples also decreased dramatically. In contrast, The T_gs and T_ms of PAW′ and P3AW′ remained almost the same as PAW and P3AW, which corresponded to enhanced photostability with A type TiO_2 nanowires.

CONCLUSIONS

In summary, TiO_2 nanofillers could be used to obtain PNA with desirable photoactivities. By incorporating 1% small size/high surface area NA TiO_2 nanoparticles into PLA, we obtained more PD PNA. On the other hand, we obtained PNA with excellent photostability by incorporating A type TiO_2 nanowires into PLA. PD PNA generated a carboxylic acid OH group and the C═C double bond after UV irradiation, whereas the spectrum of PS nanocomposites remained the same. The thermal decomposition and phase transition temperatures of PD nanocomposites were greatly reduced after UV irradiation, whereas that of PS nanocomposites remained similar. Results from this study provide a promising approach for rational design of PNA for either short-term or durable applications.

ACKNOWLEDGMENTS

Contribution No. 14-045-J from the Kansas Agricultural Experiment Station.

REFERENCES

1. Lim, L.; Auras, R.; Rubino, M. *Prog. Polym. Sci.* **2003**, *33*, 820.
2. Rasal, R.; Janorkar, A.; Hirt, D. *Prog. Polym. Sci.* **2010**, *35*, 338.
3. Li, Y.; Sun, X. *Biomacromolecules* **2010**, *11*, 1847.
4. Li, Y.; Sun, X. S. *J. Appl. Polym. Sci.* **2011**, *121*, 589.
5. Tsuji, H.; Echizen, Y.; Saha, S.; Nishimura, Y. *Macromol. Mater. Eng.* **2005**, *290*, 1192.
6. Nakayama, N.; Hayashi, T. *Polym. Degrad. Stabil.* **2007**, *92*, 1255.
7. Sakai, W.; Tsutsumi, N. In Poly(lactic acid): Synthesis, Structures, Properties, Processing, and Applications; Auras, R.; Lim, L.; Selke, S.; Tsuji, H., Eds.; John Wiley & Sons, Hoboken, New Jersey, **2010**.
8. Shogren, R.; Doane, W.; Garlotta, D.; Lawton, J.; Willett, J. *Polym. Degrad. Stabil.* **2003**, *79*, 405.
9. Hanaor, D.; Sorrell, C. *J. Mater. Sci.* **2011**, *46*, 855.
10. Fox, M. A.; Dulay, M. T. *Chem. Rev.* **1993**, *93*, 341.
11. Zhang, H. F. Banfield, J. *J. Mater. Chem.* **1998**, *8*, 2073.
12. Li, Y.; Liu, J.; Jia, Z. *Mater. Lett.* **2006**, *60*, 1753.
13. Zhang, J.; Xu, Q.; Feng, Z.; Li, M.; Li, C. *Angew. Chem.-Int. Ed.* **2008**, *47*, 1766.
14. Batzill, M.; Morales, E. H.; Diebold, U. *Phys. Rev. Lett.* **2006**, *96*, 026103.
15. Ohtani, B.; Ogawa, Y.; Nishimoto, S. *J. Phys. Chem. B* **1997**, *101*, 3746.
16. Zan, L.; Wang, S.; Fa, W.; Hu, Y.; Tian, L.; Deng, K. *Polymer* **2006**, *47*, 8155.
17. Zan, L.; Fa, W. J.; Wang, S. L. *Environ. Sci. Technol.* **2006**, *40*, 1681.
18. Miyauchi, M.; Li, Y.; Shimizu, H. *Environ. Sci. Technol.* **2008**, *42*, 4551.
19. Chen, X.; Wang, Z.; Liao, Z.; Mai, Y.; Zhang, M. *Polym. Test.* **2007**, *26*, 202.
20. Zhang, Y.; Li, G.; Jin, Y.; Zhang, Y.; Zhang, J.; Zhang, L. *Chem. Phys. Lett.* **2002**, *365*, 300.
21. Li, Y.; Venkateshan, K.; Sun, X. S. *Polym. Int.* **2010**, *59*, 1099.
22. Liu, J.; Li, J.; Sedhain, A.; Lin, J.; Jiang, H. *J. Phys. Chem. C* **2008**, *112*, 17127.
23. Yuan, Z.; Su, B. *Colloid. Surf. A* **2004**, *241*, 173.
24. Zhang, Q.; Gao, L.; Guo, J. *Appl. Catal. B* **2000**, *26*, 207.
25. Yang, H. Y.; Zhu, S. K.; Pan, N. *J. Appl. Polym. Sci.* **2004**, *92*, 3201.
26. Wypych, G. Handbook of UV Degradation and Stabilization; ChemTec Publishing: Toronto, **2011**.
27. Anpo, M.; Takeuchi, M. *J. Catal.* **2003**, *216*, 505.
28. Klabunde, K.; Richards, R. Nanoscale Materials in Chemistry; John Wiley & Sons, Inc: Hoboken, New Jersey, **2009**.
29. Kudo, A.; Omori, K.; Kato, H. *J. Am. Chem. Soc.* **1999**, *121*, 11459.
30. Bansal, A.; Yang, H.; Li, C.; Cho, K.; Benicewicz, B.; Kumar, S.; Schadler, L. *Nat Mater* **2005**, *4*, 693.